Observation of Relativistic Effects in Collective Thomson Scattering

J. S. Ross,[1,2] S. H. Glenzer,[1] J. P. Palastro,[1] B. B. Pollock,[1,2] D. Price,[1] L. Divol,[1] G. R. Tynan,[2] and D. H. Froula[1]

[1]Lawrence Livermore National Laboratory, P.O. Box 808, Livermore, California 94551, USA

[2]Mechanical and Aerospace Engineering Department, University of California at San Diego, 9500 Gilman Drive, La Jolla, California 92093-0411, USA

(Received 29 October 2009; published 10 March 2010)

We observe relativistic modifications to the Thomson scattering spectrum in a traditionally classical regime: $v_{\rm osc}/c = eE_0/cm\omega_0 \ll 1$ and $T_e < 1$ keV. The modifications result from scattering off electron-plasma fluctuations with relativistic phase velocities. Normalized phase velocities v/c between 0.03 and 0.12 have been achieved in a N_2 gas-jet plasma by varying the plasma density from 3×10^{18} cm^{-3} to 7×10^{19} cm^{-3} and electron temperature between 85 and 700 eV. For these conditions, the complete temporally resolved Thomson scattering spectrum including the electron and ion features has been measured. A relativistic treatment of the Thomson scattering form factor shows excellent agreement with the experimental data.

DOI: 10.1103/PhysRevLett.104.105001 PACS numbers: 52.25.Os, 52.27.Ny, 52.35.Fp, 52.70.Kz

Thomson scattering [1–3] is an important diagnostic for determining the plasma conditions and studying collective plasma-wave behavior in laser-produced [4–6], tokamak [7–9], and pinch [10,11] plasmas. Each of these systems can be vulnerable to plasma instabilities which are a strong function of the plasma conditions. An example is inertial confinement fusion (ICF) targets for the National Ignition Facility (NIF) [12] which require a detailed understanding of the plasma temperature and density in order to mitigate laser-plasma instabilities [13]. The high-density conditions accessible at laser facilities present a new regime for collective Thomson scattering where understanding relativistic effects is essential.

Collective Thomson scattering is the scattering of light from electron-density fluctuations with a wave vector $\mathbf{k}$ whose inverse is larger than the Debye length ($k\lambda_D < 1$). Therefore, collective scattering probes fluctuations corresponding to the natural modes of the plasma and the spectra contain four distinct features, corresponding to ion-acoustic and electron-plasma resonances. Light scattered from the co- and counterpropagating modes is redshifted and blueshifted by the frequency of the resonance, and the intensity of the scattered light is in general governed by the Landau damping of each mode. Therefore, the frequency and shape of the scattered spectrum can be an accurate measure of the plasma parameters. A majority of Thomson scattering experiments [4–6] have resolved the ion-acoustic feature to provide an accurate measure of the electron temperature. Scattering from the electron-plasma resonance is ideal for measuring the electron density, but has seen limited application in the collective regime due to the small scattering cross section.

For noncollective Thomson scattering ($k\lambda_D > 1$), where the light is scattered by free electrons, relativistic effects governed by the thermal velocity of the electrons [14,15] have been observed [16]. Relativistic nonlinear effects due to extremely high Thomson scattering probe intensities ($>10^{18}$ W cm^{-2}) causing relativistic electron motion have been measured [17]. Previous collective-scattering measurements from electron-plasma waves [18] have only resolved the redshifted resonance, making characterization of relativistic effects difficult. There have been no definitive measurements of relativistic effects from thermal fluctuations.

In this Letter, we present the first observation of a relativistic correction to the thermal collective Thomson scattering spectrum. We measure a factor of $1/2$ difference between the blueshifted electron-plasma-wave resonance peak power calculated using the nonrelativistic Thomson scattering form factor and the measured peak power for a normalized phase velocity of $\beta = \omega/kc = 0.12$. This result is attributed to two effects: (1) the relativistic aberration of light which causes a source that emits uniformly in the rest frame to preferentially emit in its direction of motion when moving relativistically, and (2) the interaction of the initial electron motion with the magnetic field of the Thomson scattering probe beam. In collective scattering, both of these effects are governed by the electrons moving near the phase velocity of the plasma wave, which can be relativistic even at low temperatures, and vary the shape of the scattering spectrum by asymmetrically changing the power scattering into the blueshifted and redshifted electron-plasma features. As the phase velocity is reduced, the relativistic correction is reduced, but is always significant for our measurements made between $\beta = 0.03$ and $\beta = 0.12$. A relativistic treatment of the scattering spectrum in the weak probe limit [19] shows excellent agreement with our measurements. An analysis of the scattering spectrum expected from ICF plasmas is performed and shows the potential error in inferred plasma conditions using a nonrelativistic scattering spectrum. Furthermore, the ion-acoustic features are simultaneously measured, and no relativistic effects at the low temperatures studied are observed or expected [20].

The experiment was performed at the Jupiter Laser Facility using the Janus Laser System. A 300 J, 527 nm (2ω), laser is focused at target chamber center (TCC) using an $f/6.7$ lens [Fig. 1(a)] where it ionizes the target gas and scatters light to the Thomson scattering diagnostic. A continuous phase plate is used to produce a 600-μm super-Gaussian focal spot. The pulse length is a 3-ns long plateau with a 150 ps rise and fall. A 1.5-mm diameter gas jet with a nitrogen backing pressure ranging from 10 to 400 psi positioned 1.0 mm below TCC provides neutral gas densities between 1.4×10^{18} cm^{-3} and 1×10^{19} cm^{-3}.

An $f/4$ collection lens collimated light scattered 90° relative to the laser beam from the Thomson scattering volume located at TCC. The scattered light is split using a 532 nm notch filter and propagated to a pair of spectrometers. The notch filter reflects light with a wavelength of 532 nm $\pm$ 10 nm which is focused onto the entrance slit of a 1-meter spectrometer using an $f/10$ focusing lens. The light transmitted through the notch filter was focused onto the entrance slit of a 1/3-meter spectrometer using an $f/10$ spherical focusing mirror. Both optical systems provide a magnification of 2.5. The 1-meter and 1/3-meter spectrometers are coupled to an S-20 and S-1 Hamamatsu streak camera, respectively. Both systems use a spectrometer entrance slit of 200 μm and a streak camera entrance slit of 400 μm. A 2400 grooves/mm grating in the 1-meter system results in a spectral resolution of 0.056 nm and a temporal resolution of 550 ps [21]. The 1/3-meter system uses a 150 grooves/mm grating resulting in a spectral resolution of 3.6 nm and a temporal resolution of 400 ps. The Thomson scattering volume 600 μm $\times$ 160 μm $\times$ 80 μm is defined by the overlap of the spectrometer and streak camera slit images at TCC with the laser beam. A spectrally calibrated Tungsten lamp inserted at TCC is used to measure the spectral intensity response of the 1/3-meter system [Fig. 1(d)]. A maximum spectral sensitivity variation of 60% is observed over the 200 nm measurement region.

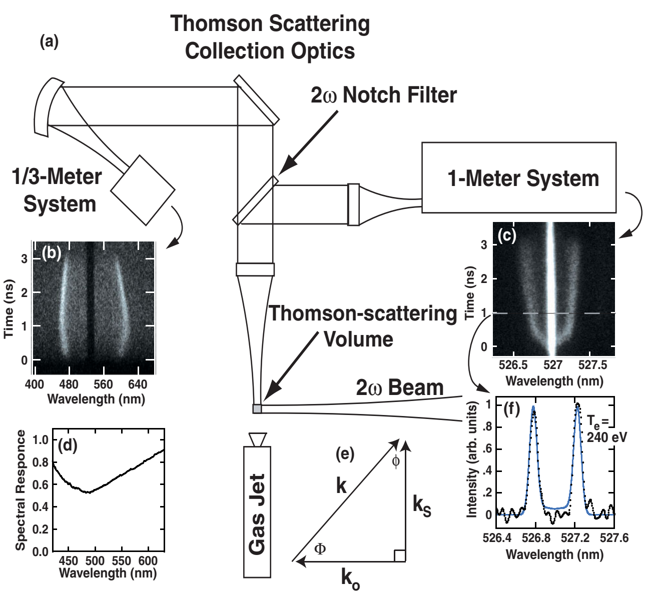

FIG. 1 (color online). (a) Experimental setup. Thomson scattered light is collected 90° relative to the laser beam. Scattering from (b) electron-plasma waves and (c) ion-acoustic waves are displayed. (d) The spectral response of the system used to measure the electron-plasma-wave spectra is characterized using a tungsten lamp. (e) The Thomson scattering k-vector diagram shows the orientation of the k vector that is probed. (f) The ion-acoustic wave spectrum (dots) at 1 ns is fit by the calculated form factor (solid line) with an electron temperature of 240 eV and a density of 1.4×10^{19} cm^{-3} after subtracting the background and stray light.

The plasma temperature has been well characterized by fitting the ion-acoustic spectra [Fig. 1(f)] with the fully relativistic form factor. The electron temperature increases rapidly over the first 100 ps and plateaus at a nearly constant temperature. At low densities (3×10^{18} cm^{-3}), the electron temperature plateaus at around 90 eV while at high densities (7×10^{19} cm^{-3}) the temperature peaks around 700 eV. The uncertainty in these measurements is better than 15% and is dominated by our uncertainties in the ion temperature which is only assumed to be less than the electron temperature.

Figure 2 shows the temporally resolved collective Thomson scattering from electron-plasma waves for various phase velocities (i.e., densities). The primary difference between the nonrelativistic and relativistic form factors is observed in the reduction of the redshifted electron-plasma-wave peak. As the normalized phase velocity of the electron-plasma-wave increases from 0.03 to 0.09, the relativistic effects become more pronounced.

A fully relativistic treatment has been developed [19] and approaches, for our low temperature conditions, a second order treatment including terms of order β^2. The form factor shows excellent agreement with the experimental data (Fig. 2). In the case where $(v_{\mathrm{th}}/c)^2 \ll 1$, scattering is measured perpendicular to the incident electric field direction, and $\beta^3 \ll 1$, the second order treatment can be written $P(k,\omega) = P_e(k,\omega) + P_i(k,\omega)$, where

$$P_e(k,\omega) = \frac{P_0 r_e^2 n_e}{2Ack} f_{e0}(\beta)\left\{\left[\left(1+\frac{\omega}{\omega_i}\right)^2 - \beta^2 + \zeta\left(\frac{\omega}{\omega_i}\right)\beta\right] \times \left|\frac{1-\chi_e}{\varepsilon}\right|^2 + \zeta\left(\frac{\omega}{\omega_i}\right)\left|\frac{\chi_e}{\varepsilon}\right|^2\beta + \beta^2\left(\frac{\omega_p}{\omega}\right)^2 \times \mathrm{Re}\left[\frac{1+\chi_i}{|\varepsilon|^2}\right] - \frac{1}{2}\beta^2\right\},$$

$$P_i(k,\omega) = \frac{ZP_0 r_e^2 n_e}{2Ack} f_{i0}(\beta)\left\{\left[\left(1+\frac{\omega}{\omega_i}\right)^2 - \beta^2 + 2\zeta\left(\frac{\omega}{\omega_i}\right)\beta\right]\left|\frac{\chi_e}{\varepsilon}\right|^2 + \beta^2\left(\frac{\omega_p}{\omega}\right)^2 \mathrm{Re}\left[\frac{\chi_e}{|\varepsilon|^2}\right]\right\}, \quad (1)$$

P_0 is the incident power, A is the cross-sectional area of the Thomson scattering volume, r_e is the classical electron radius, n_e is the electron density, $\varepsilon = 1 + \chi_e + \chi_i$ is the dielectric function, χ_e, χ_i is the electron, ion susceptibility, respectively, Z is the average ionization state, $f_{e0}(\beta)$ and

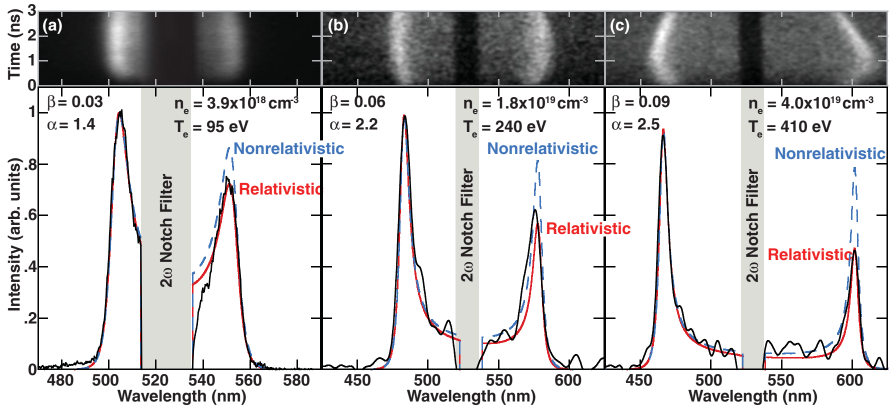

FIG. 2 (color online). Top panels: raw streak data. Bottom panels: experimental data (solid-black line) at 2 ns normalized to the blueshifted feature and compared to the nonrelativistic (blue-dashed line) and relativistic (solid-red line) form factors. As the temperature and density increase, the phase velocity of the electron-plasma-wave increases (a) $\beta = 0.03$, (b) $\beta = 0.06$, (c) $\beta = 0.09$ and the difference between the nonrelativistic and relativistic form factors becomes more pronounced.

$f_{i0}(\beta)$ are the one-dimensional Maxwellian distributions for electrons and ions, respectively, $\omega = \omega_s - \omega_i$, ω_s is the scattered frequency, ω_i is the incident frequency, $\zeta = (\hat{k} \cdot \hat{k}_s)$, and $\hat{k}_s$ is the unit vector from the source to the detector.

For our conditions, the relativistic effects are observed in the asymmetric scattering spectrum and attributed to two effects, corresponding to first order in beta corrections to the calculated scattered spectrum. The first effect is due to relativistic aberration, also referred to as the relativistic "headlight" effect, where light is preferentially directed in the emitter's direction of propagation [22]. The second effect is a result of the relativistic motion of the electrons involved in the scattering with the magnetic field of the Thomson scattering probe laser. The resulting $\vec{v} \times \vec{B}$ force, which is neglected in the nonrelativistic treatment, is in the same direction as the force of the incident electric field. When the electron is moving towards the detector, the increased force on the electron enhances the scattered power. When the electron is moving away from the detector the force is in the opposite direction and the scattered power is reduced. The effects of these corrections can be estimated by taking the ratio of the peak power in the blueshifted and redshifted electron-plasma-wave resonances,

$$\frac{P^{\text{blue}}}{P^{\text{red}}} \approx \underbrace{\frac{P_{\text{nr}}^{\text{blue}}}{P_{\text{nr}}^{\text{red}}}}_{A} \underbrace{\frac{(1+\beta\cos\phi)^2}{(1-\beta\cos\phi)^2}}_{B} \underbrace{\frac{(1+\beta\cos\Phi)^2}{(1-\beta\cos\Phi)^2}}_{C}, \tag{2}$$

where ϕ is the angle between $\hat{k}$ and $\hat{k}_S$, Φ is the angle between $\hat{k}$ and $\hat{k}_0$, both of which are shown in Fig. 1(e) and equal 45° for our scattering geometry, and

$$P_{\text{nr}}(k,\omega) = \frac{P_0 r_e^2 n_e}{2Ack}\left[\left|\frac{1+\chi_i}{\varepsilon}\right|^2 f_{e0}(\beta) + Z\left|\frac{\chi_e}{\varepsilon}\right|^2 f_{i0}(\beta)\right], \tag{3}$$

is the nonrelativistic Thomson scattered power spectrum [1–3]. Equation (3) is recovered from Eq. (1) by letting terms of order $\beta^2 = \omega/\omega_i = 0$. The asymmetry in term A of Eq. (2) is due to Landau damping, term B is due to relativistic aberration, and term C is due to the initial particle motion interacting with the magnetic field.

Figure 3 shows agreement between the experimental data and the form factor including relativistic corrections [Eq. (1)] for normalized phase velocities ranging from 0.03 to 0.12. The data are compared with calculations using the nonrelativisitc power spectrum [Eq. (3)] where the asymmetry in the peaks is given by the Landau damping. When using a simple model to correct for the relativistic effects [Eq. (2)], the scattered power agrees with the fully relativistic form factor. The spectra are normalized to the peak

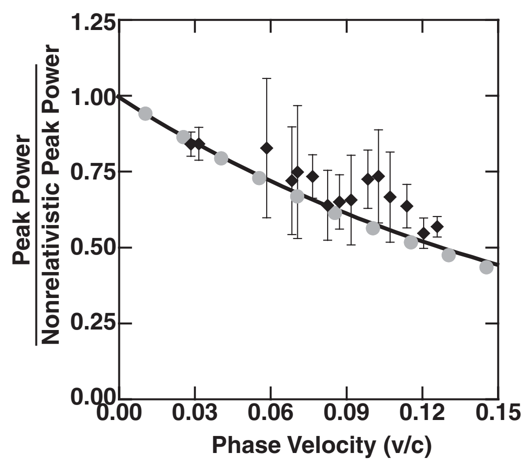

FIG. 3. The measured peak powers in the redshifted feature are divided by the calculated peak powers [Eq. (3), diamonds] and are plotted as a function of phase velocity. The electron temperature ranged from 85 to 720 eV. Data in perfect agreement with the nonrelativistic form factor would have a value of unity. The ratio of the relativistic peak power (solid line) and the corrected nonrelativistic peak power [Eq. (2), gray circles] divided by the nonrelativistic peak power are shown.

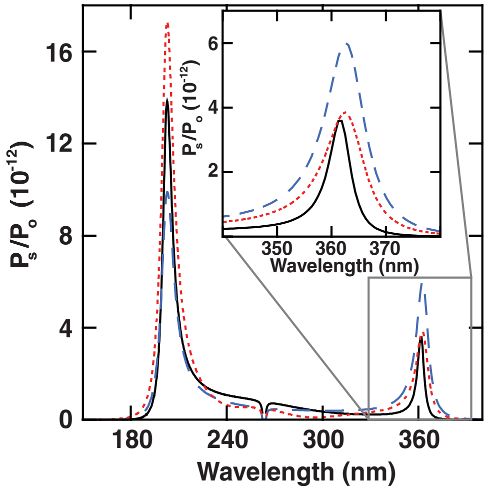

FIG. 4 (color online). The nonrelativistic [Eq. (3), blue-dashed line], second order relativistic [Eq. (1), red-dotted line] and fully relativistic (solid-black line) form factors are compared for typical plasma conditions on the NIF: an electron temperature of 10 keV, electron density of 8.0×10^{20} cm^{-3}, and a scattering angle of 35° using a Thomson scattering probe beam with a wavelength of 263.5 nm. These conditions result in a normalized electron-plasma-wave phase velocity of 0.37.

power in the blueshifted feature (see Fig. 2) and fit using the form factors. The measured peak scattered power in the redshifted feature divided by the peak scattered power calculated using the nonrelativistic form factor is plotted in Fig. 3. Thomson scattered light is observed for the full 3-ns duration of the laser beam (Fig. 2), after 1 ns the electron temperature and density are determined at 250 ps intervals by fitting Eq. (1) to the measured spectrum. The measured spectra are obtained by integrating over a 200 ps region. For clarity we average multiple shots at a particular phase velocity; the error bars represent twice the standard deviation within this average. Small discrepancies for some shots are due to noise.

Fitting the ion-acoustic spectrum with Eqs. (1) and (3) shows that relativistic corrections are not important for scattering from the ion-acoustic resonances at our conditions. Discrepancies are not expected until the phase velocity of the ion-acoustic wave is greater than 1% of the speed of light which is estimated to be when $T_e \approx 140$ keV assuming $ZT_e \gg 3T_i$ and a fully ionized nitrogen plasma.

Figure 4 compares the nonrelativistic form factor [Eq. (3)], a relativistic form factor including terms of second order in β [Eq. (1)], and the fully relativistic form factor for typical NIF conditions. Notice that for collective high-temperature conditions the asymmetry between the different form factors is pronounced and a 2 nm wavelength shift resulting from the relativistic Maxwellian distribution used to evaluate the fully relativistic form factor is observed. Neglecting the relativistic frequency shift produces a 13% error in the measured electron temperature and a 5% error in the measured electron density for the conditions shown in Fig. 4.

In conclusion, we have measured relativistic effects in collective Thomson scattering from electron-plasma waves which are attributed to the relativistic "headlight" effect and the electron motion in the direction of the incident light vector interacting with the magnetic field of the Thomson scattering probe. A relativistic form factor shows excellent agreement with the measured spectra and is required to accurately analyze scattering from electron-plasma waves in most laser-produced plasmas where T_e and n_e are greater than 100 eV and 1.0×10^{19} cm^{-3}, respectively. These results will affect future high-energy density laboratory plasma experiments where relativistic effects must be taken into account when scattering from electron-plasma waves even at nonrelativistic temperatures. In addition, relativistic effects on the growth of collective plasma waves by parametric laser-plasma instabilities must be examined at high phase velocities.

I would like to acknowledge contributions from J. Sheffield and C. Clayton. This work was performed under the auspices of the U.S. Department of Energy by Lawrence Livermore National Laboratory under Contract No. DE-AC52-07NA27344 and was partially funded by the Laboratory Directed Research and Development Program under project tracking code 08-LW-070.

[1] J. A. Fejer, Can. J. Phys. **38**, 1114 (1960).
[2] J. Sheffield, *Plasma Scattering of Electromagnetic Radiation* (Academic, New York, 1975).
[3] I. H. Hutchinson, *Principles of Plasma Diagnostics* (Cambridge University Press, Cambridge, 1987).
[4] S. H. Glenzer *et al.*, Phys. Rev. Lett. **79**, 1277 (1997).
[5] D. H. Froula, L. Divol, and S. H. Glenzer, Phys. Rev. Lett. **88**, 105003 (2002).
[6] D. H. Froula *et al.*, Phys. Plasmas **10**, 1846 (2003).
[7] N. Peacock *et al.*, Nature (London) **224**, 488 (1969).
[8] R. Behn *et al.*, Phys. Rev. Lett. **62**, 2833 (1989).
[9] F. Alladio *et al.* Phys. Lett. A **60**, 39 (1977).
[10] T. Wrubel *et al.*, Plasma Phys. Controlled Fusion **42**, 519 (2000).
[11] R. Pasqualotto *et al.*, Rev. Sci. Instrum. **70**, 1416 (1999).
[12] J. D. Lindl *et al.*, Phys. Plasmas **11**, 339 (2004).
[13] H. Baldis *et al.*, Phys. Rev. Lett. **80**, 1900 (1998).
[14] R. Pechacek *et al.*, Phys. Fluids **10**, 1688 (1967).
[15] H. Bindslev, Plasma Phys. Controlled Fusion **33**, 1775 (1991).
[16] M. Mattioli *et al.*, Plasma Phys. Controlled Fusion **17**, 165 (1975).
[17] S. Chen *et al.*, Nature (London) **396**, 653 (1998).
[18] S. H. Glenzer *et al.*, Phys. Rev. Lett. **82**, 97 (1999).
[19] J. P. Palastro *et al.*, Phys. Rev. E (to be published).
[20] J. Zheng and C. X. Yu, Plasma Phys. Controlled Fusion **51**, 095009 (2009).
[21] A. Visco *et al.*, Rev. Sci. Instrum. **79**, 10F545 (2008).
[22] E. F. Taylor and J. A. Wheeler, *Spacetime Physics* (W. H. Freeman and Company, San Francisco and London, 1966).